

# X-ray fluorescence and visible near infrared sensor fusion for predicting soil chromium content

Dongyun Xu<sup>a</sup>, Songchao Chen<sup>b</sup>, R.A. Viscarra Rossel<sup>c</sup>, Asim Biswas<sup>d</sup>, Shuo Li<sup>e</sup>, Yin Zhou<sup>a</sup>, Zhou Shi<sup>a,f,g,\*</sup>

<sup>a</sup> Institute of Agricultural Remote Sensing and Information Technology Application, College of Environmental and Resource Sciences, Zhejiang University, Hangzhou 310058, China

<sup>b</sup> INRA, Unité InfoSol, 45075 Orléans, France

<sup>c</sup> School Molecular & Life Sciences, Curtin University, 6102 Bentley, Australia

<sup>d</sup> School of Environmental Sciences, University of Guelph, 50 Stone Road East, Guelph, ON N1G 2W1, Canada

<sup>e</sup> College of Urban and Environmental Sciences, Central China Normal University, Wuhan 430079, China

<sup>f</sup> Key Laboratory of Spectroscopy Sensing, Ministry of Agriculture, Hangzhou, China

<sup>g</sup> State Key Laboratory of Soil and Sustainable Agriculture, Institute of Soil Science, Chinese Academy of Sciences, Nanjing, China

## ARTICLE INFO

Handling Editor: Alex McBratney

### Keywords:

Outer-product analysis

Granger–Ramanathan averaging

Proximal soil sensor

Soil spectroscopy

## ABSTRACT

Anthropogenic activities, such as sewage irrigation and application of pesticides and fertilizers, are the main cause of chromium (Cr) contamination in agricultural soils. Cr contamination reduces soil quality and threatens environmental and human health. Conventional Cr measurement methods, although accurate, involve complex sample processing steps and sophisticated laboratory analysis, which are time-consuming, costly, and often environmentally unfriendly. X-ray fluorescence (XRF) and visible near-infrared (vis-NIR) spectroscopy have been recognized as alternatives to measure soil heavy metal contamination in a cheap, fast, non-destructive, and environmentally conscious manner. In this study, 301 paddy soil samples from Fuyang, Zhejiang Province, China were used to explore the feasibility and effectiveness of XRF and vis-NIR spectra separately and in combination for estimating the soil Cr content. Two strategies, including outer-product analysis (OPA) and Granger–Ramanathan averaging (GRA), were used to combine the spectra and spectral models, respectively, from the two instruments (sensor fusion). Partial least-squares regression (PLSR) was used to train the models using a single sensor (XRF or vis-NIR spectra) and OPA fused spectra. Fifty boot straps were used to assess the uncertainty of the predictions for the aforementioned models. The results indicated that XRF spectra performed better than vis-NIR spectra for predictions of Cr content, with a Lin's concordance correlation coefficient ( $\rho_c$ ) of 0.83, a root mean square error (RMSE) of 8.80, and a ratio of prediction derivation (RPD) of 1.75. Sensor fusion by OPA gave the highest prediction accuracy with a  $\rho_c$  of 0.90, RMSE of 6.80, and RPD of 2.30. The sensor fusion by GRA gave similar results with a  $\rho_c$  of 0.88, RMSE of 7.40, and RPD of 2.13. The predictions using both methods (OPA and GRA) were acceptable when considering the standard deviation of differences (SDD = 4.23). This suggests that OPA and the GRA sensor fusion methods are efficient and accurate for rapid measurement of Cr and provide a way forward for using these technologies for fast, sensor-based soil characterization.

## 1. Introduction

Chromium (Cr) is widely distributed in soils and rocks. The two main valence states for Cr in soils are Cr(III) and Cr(VI) (Di Palma et al., 2015). The Cr(VI) state is toxic and can be taken up by plants, accumulated in plants, and be absorbed by humans where it has carcinogenic effects (Ellis et al., 2002). Over the past decades, Cr

contamination in soils has increased with the rapid increase of population and industry (Gao and Xia, 2011). Environmental protection agencies in many countries, including the United States Environmental Protection Agency, have ranked Cr as a priority soil pollutant (Juvera-Espinosa et al., 2006; Fernández et al., 2010). Therefore, it is critical to better characterize the soil Cr content to understand its effects and associated environmental issues that could affect humans.

\* Corresponding author at: Institute of Agricultural Remote Sensing and Information Technology Application, College of Environmental and Resource Sciences, Zhejiang University, Hangzhou 310058, China

E-mail address: [shizhou@zju.edu.cn](mailto:shizhou@zju.edu.cn) (Z. Shi).

<https://doi.org/10.1016/j.geoderma.2019.05.036>

Received 17 January 2019; Received in revised form 21 May 2019; Accepted 23 May 2019

0016-7061/© 2019 Elsevier B.V. All rights reserved.

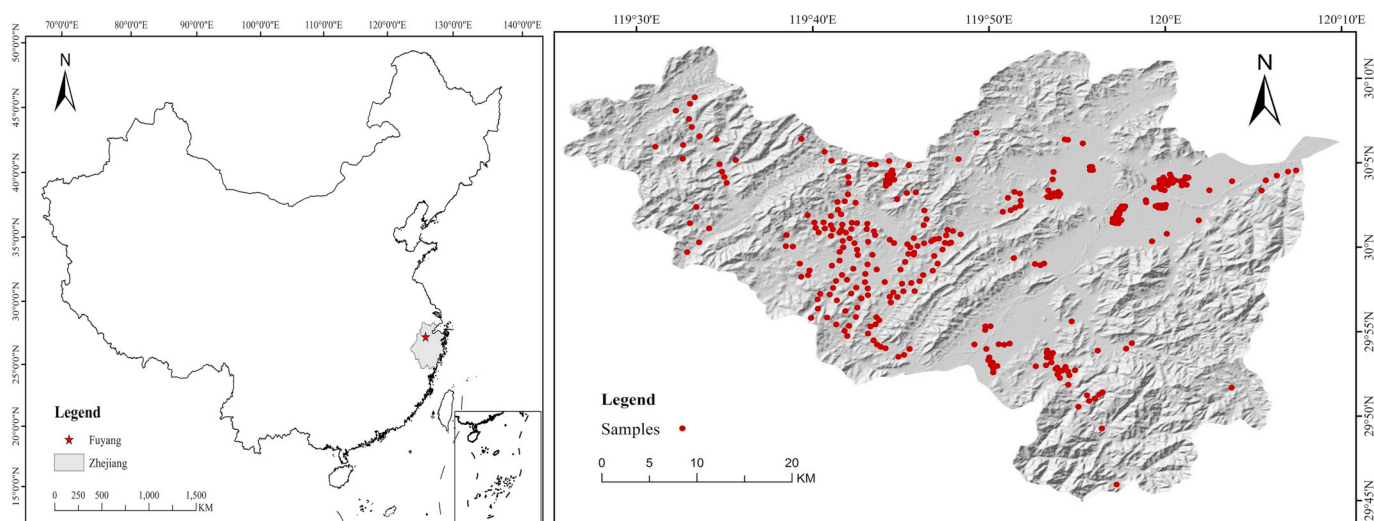


Fig. 1. Study area and soil sampling sites. Zhejiang province and Fuyang are labeled with grey and red stars, respectively. Sampling sites are marked with red circles in the right figure. (For interpretation of the references to color in this figure legend, the reader is referred to the web version of this article.)

Traditionally, the measurement of soil heavy metal content requires field sampling followed by wet chemical digestion and inductively coupled plasma (ICP) or atomic absorption spectrometry (AAS) analyses. Soil sampling and wet chemical digestion are usually labor-intensive, time-consuming, costly, and often environmentally unfriendly. Because of these challenges, traditional methods are limited to specific sampling sites and they are unable to provide spatial variations of Cr contamination quickly over large areas (Shi et al., 2014). Therefore, rapid, accurate, and environmentally friendly techniques are needed for the determination of soil Cr. And improvements in analytical techniques also provides an opportunity to increase sampling density, which will be helpful for obtaining a more detailed understanding of spatial variations and improving decision making. More recently, proximal soil sensing techniques, such as X-ray fluorescence spectroscopy (XRF) and visible and near-infrared (vis–NIR) spectroscopy, have gained the attention of researchers for rapid characterization of soil.

X-ray fluorescence spectroscopy (XRF) has become increasingly popular for its high sample throughput and minimal sample preparation (Zhu et al., 2011). It provides accurate total elemental contents of soils in a short time (Reidinger et al., 2012), and especially useful for the measurement of heavy metal content in soils (O'Rourke et al., 2016; Caporale et al., 2018). It can be used for rapid, cost-effective, and simple monitoring of contaminated soils. Moreover, XRF is applicable both under laboratory and field conditions as it creates no toxic waste, which is beneficial compared with traditional laboratory analysis.

Similarly, visible and near-infrared (vis–NIR) spectroscopy has been widely applied in the evaluation of soil properties, such as soil organic matter, clay minerals and iron oxides (Shi et al., 2015; Ji et al., 2015; Xu et al., 2018), because it is cheap, fast, effective, non-destructive, and environmentally friendly (Stenberg et al., 2010; Viscarra Rossel et al., 2016; Chen et al., 2019a). Some researchers have also investigated vis–NIR for the measurement of soil heavy metal contents (Shi et al., 2014; Horta et al., 2015; Chakraborty et al., 2017). Although there are no direct spectral features for heavy metals such as Cr in the vis–NIR regions (Baveye and Laba, 2015), heavy metals are often bound to soil components such as iron oxides, clay minerals, and organic matter (Choe et al., 2008; Chen et al., 2015; Shi et al., 2016). Thus, there is a close relationship between heavy metals and these soil components that do have direct responses in the vis–NIR region of the electromagnetic spectrum (Piccolo and Stevenson, 1982). Previous studies have shown the potential of vis–NIR spectroscopy for indirect measurements of heavy metals with reliable prediction accuracy (Kemper and Sommer, 2002; Sun et al., 2018).

Despite the advantages of being rapid and convenient, XRF and vis–NIR spectroscopic predictions of soil properties often suffer from a high degree of uncertainty, which is mostly caused by soil sample heterogeneity (Argyaki et al., 1997; Hou et al., 2004). Therefore, integrated applications of proximal soil sensing techniques such as XRF and vis–NIR, and vis–NIR and MIR have been tested to improve the prediction accuracy (Viscarra Rossel et al., 2006; Wang et al., 2015; O'Rourke et al., 2016; Xu et al., 2019). Generally, the main methods for integration of sensors are data integration (e.g., outer product analysis, OPA) and model integration (e.g., model averaging). OPA is a method which makes it possible to emphasize co-evolution of spectral regions in signals obtained from two different spectra or even from the same spectrum (Jaillais et al., 2006; Barros et al., 2008). Therefore, OPA can combine spectra from different sensors and analyze their mutual variations caused by different concentrations of components in soil samples (Vesela et al., 2007; Terra et al., 2019). The applications of OPA are mainly in food science (Jaillais et al., 2006; Vesela et al., 2007) with a recent application in soil science (Terra et al., 2019). Application of OPA in combining XRF and vis–NIR spectra of soil samples has yet to be explored. Another method of sensor fusion, combining different model outcomes into a new one, is known as model averaging or ensemble modelling (Rojas et al., 2008). The model averaging approach has shown potential for improving the prediction accuracy compared with single sensor models in various scales (Malone et al., 2014; O'Rourke et al., 2016; Xu et al., 2019). Among the different model averaging methods, Granger–Ramanathan Averaging (GRA) is simple and efficient, and it has been used in several digital soil mapping and spectroscopic prediction studies (Malone et al., 2014; O'Rourke et al., 2016; Chen et al., 2019b).

The objective of this study was to predict soil Cr content using XRF and vis–NIR spectra and to compare the Cr prediction accuracies using individual sensors, data integration (i.e., OPA) and model integration (i.e., GRA).

## 2. Materials and methods

### 2.1. Study site and soil sampling

Our study area was located in Fuyang, which is in the southern part of the Yangtze River Delta, Zhejiang Province, China, and covered an area of 1831 km<sup>2</sup> (Fig. 1). The main soil type in this area is paddy soil, a kind of Anthrosols in Chinese Soil Taxonomy (Gong et al., 2007). Grid soil sampling was conducted in the cropland, which was extracted from

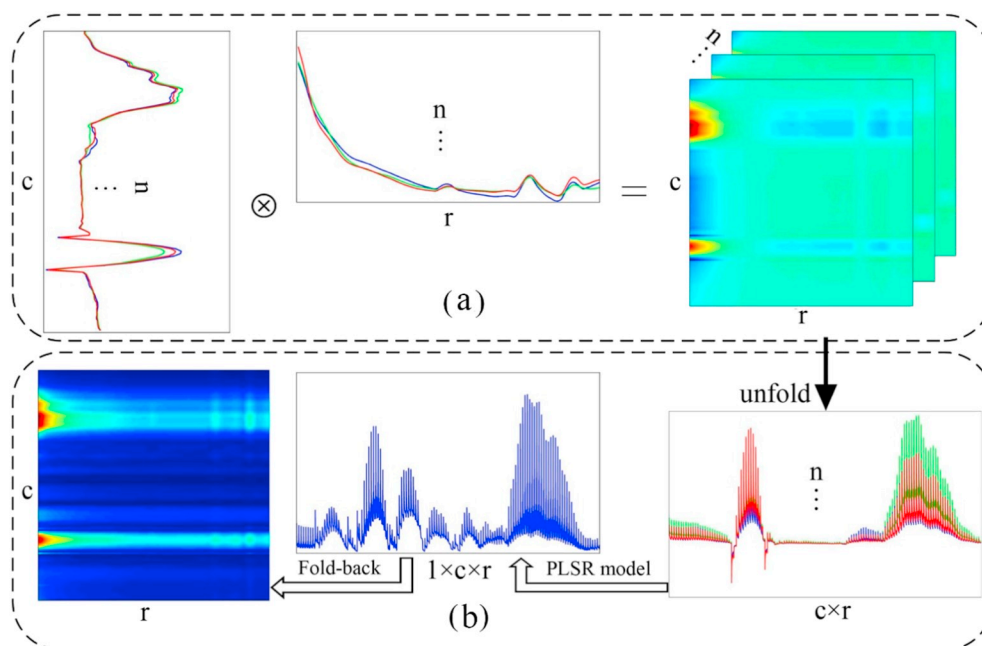


**Fig. 2.** Process of data fusion by OPA (a) and the unfolding process for modelling and refolding of the model results (b) (revised after Jaillais et al., 2005).  $c$  is the number of variables for XRF and  $r$  is the number of wavelengths for vis-NIR,  $n$  is the number of soil samples.

land use maps. For cropland located far away from the town, soil samples were chosen by a contiguous area of 1 km<sup>2</sup>; for cropland located near the town, the grid area was set to about 0.16 km<sup>2</sup>. A total of 301 sampling sites were selected, and for each site, five individual topsoil samples (0–20 cm) were collected and composited to form one representative sample. The soil samples were air-dried, and stones and roots were removed by hand. The samples were then divided into two parts, and one part was ground and sieved to < 2 mm for spectral measurements and the other part was sieved to < 0.15 mm for laboratory chemical analysis (Technical Specification for soil Environmental monitoring (HJ/T 166-2004), [http://kjs.mep.gov.cn/hjbhzbz/bzwb/jcffbz/200412/t20041209\\_63367.shtml](http://kjs.mep.gov.cn/hjbhzbz/bzwb/jcffbz/200412/t20041209_63367.shtml)).

## 2.2. Laboratory chemical analysis

Ground and sieved soil samples were pre-processed by the microwave digestion method using 4 mL of HNO<sub>3</sub> (65.0%), 2 mL of HCl (36.0%), and 2 mL of HF (40.0%). The soil Cr content was then measured using Liquid chromatography inductively coupled plasma mass spectrometer (LC-ICP-MS) (NexION 300 X, PerkinElmer, Inc., USA). Certified soil reference materials (GBW07405, GBW07407, GBW07447, and GBW07451; National Research Centre for Certified Reference Materials of China) were used to verify the accuracy of the LC-ICP-MS method. About 15% of the soil samples were analyzed twice to evaluate the repeatability of the method.

## 2.3. Measurement of vis-NIR and XRF spectra

The vis-NIR spectra of the soil samples were recorded using a Fieldspec® Pro FR vis-NIR spectrometer (PANalytical Inc., formerly Analytical Spectral Devices-ASD, Boulder, CO) with a spectral range of 350–2500 nm. The instrument has a spectral resolution of 3 nm between 350 and 1000 nm, and a spectral resolution of 10 nm between 1000 and 2500 nm. The sampling resolution of the spectra is 1 nm. Before each measurement, a Spectralon® panel with 99% reflectance was used to calibrate the spectrometer. Then soil samples were measured using a high-intensity contact probe (PANalytical Inc.) with its own light source. Three random measurements were scanned at different positions in a petri dish (10 cm in diameter and 1 cm high). At

each measurement, the instrument recorded 10 internal scans for a satisfactory signal-to-noise ratio. A total of 30 spectra were averaged into one spectrum to represent the sample.

The XRF spectra were collected using a Thermo Fisher Scientific Niton™XL2 GOLDD analyser (Thermo Fisher Scientific Inc., Billerica, MA, USA). The instrument was calibrated against a background for every 30 samples. ‘Soils Mode’ was chosen for the XRF spectral measurements, and each sample was scanned three times for 90 s each time. Finally, the average of the three measurements was taken as the spectra of the sample. The limits of detection (LODs) of XL2 GOLDD analyser for Cr is 70 ppm. After measurement, only 138 samples had Cr concentration (derived from XRF) among 301 samples, and the remaining samples were lower than the LODs. Therefore, we did not use the Cr elemental concentrations from XRF and only used XRF spectra for this study.

## 2.4. Spectral pre-processing

The vis-NIR spectra were first reduced to 400–2450 nm to eliminate the influence of noise and then transformed into absorbance using  $\log(1/R)$  ( $R$  is the reflectance). The spectra were then smoothed by the Savitzky-Golay algorithm (SG; Savitzky and Golay, 1964) to further reduce the noise and enhance the signal, with a window size of 15 and polynomial of order 2. The XRF spectra were reduced to 0.405–42.105 keV to eliminate the low energy spectra and then smoothed by SG with a window size of 13 and polynomial of order 2. Then vis-NIR and XRF spectra were down-sampled to a resolution of 10 nm and 0.15 keV respectively, to reduce redundancy and improve the modelling efficiency. Before chemometric analysis, the outliers in the Cr measurements and XRF and vis-NIR spectra were identified using principal component analysis and boxplots, and the remaining 291 samples were used to conduct the modelling.

## 2.5. Sensor fusion: outer-product analysis algorithm

Outer-product analysis (OPA) is a method that combines two kinds of spectra and uses their combinations to emphasize co-evolution of spectral regions (Jaillais et al., 2005). For example (Fig. 2), in the OPA process, we have  $c$  number of variables for XRF and  $r$  number of wavelengths for vis-NIR with  $n$  number of soil samples scanned using each

instrument. The combinations (vis–NIR  $\otimes$  XRF) will produce  $n$  outer product matrices ( $c$  rows by  $r$  columns) with the multiplied intensities of the original two domains (Fig. 2a). Then, the  $c \times r$  matrix is unfolded to a  $c \times r$  vector and this produces a new matrix with  $n$  rows and  $c \times r$  columns for chemometric analysis, such as partial least squares regression (PLSR). After the chemometric analysis, the related result, such as variable importance in projection (VIP) value ( $c \times r$  vector) is folded-back to the outer-product matrix ( $c$  rows with  $r$  columns) which will make it easy to explain and interpret the model (Fig. 2b; Jaillais et al., 2005; Barros et al., 2008; Terra et al., 2019). The steps of OPA were implemented in R 3.3.3 (R Core Team, 2017).

## 2.6. Model construction and assessment

We used the Rank-KS algorithm (Kennard and Stone, 1969; Chen et al., 2016) to split the calibration and validation data. This involved sorting the data by the Cr content in ascending order, dividing the data into six blocks, and implementing the Kennard-Stone algorithm (Kennard and Stone, 1969) in each block (Xu et al., 2018). Two thirds of the entire data were chosen as calibration data.

### 2.6.1. The PLSR algorithm

Among the multiple linear calibration algorithms, PLSR is one of the most popular algorithms for spectral calibration and prediction (Wold et al., 1983). This method has the advantage of eliminating the problem of multiple collinearities of independent variables (Næsset et al., 2005). In this study, PLSR was performed in the ‘pls’ package (Mevik and Wehrens, 2016) of R 3.3.3 (R Core Team, 2017). To evaluate the relative importance of each waveband in the projection used in each of the PLSR models, VIP scores (Wold et al., 2001) were used to determine important wavelengths used in the PLSR calibration. This was carried out in PLS\_Toolbox 8.5.1 (Eigenvector Research Inc., Wenatchee, WA, USA) in MatLab (The MathWorks Inc., Natick, MA, USA).

### 2.6.2. The GRA algorithm

Granger–Ramanathan averaging (GRA) was used to combine the single sensor prediction results from XRF and vis–NIR. This algorithm uses ordinary least squares to combine different outcomes (Granger and Ramanathan, 1984). It fits a multiple linear regression model where measured values are regressed against the corresponding predictions derived from the different sensor predictions. We implemented this in R 3.3.3 (R Core Team, 2017).

$$Y = W_0 + (W_{XRF} \times X_{XRF}) + (W_{vis-NIR} \times X_{vis-NIR}) \quad (1)$$

where  $Y$  is the vector with the soil property of interest (i.e., Cr content);  $X_{XRF}$  and  $X_{vis-NIR}$  are the independent variables (prediction outcomes of XRF and vis–NIR),  $W_0$  is the intercept; and  $W_{XRF}$  and  $W_{vis-NIR}$  are the weights of the XRF and vis–NIR outcomes, respectively.

### 2.6.3. Uncertainty analysis

To improve the robustness of the models and quantify the uncertainty of the predictions, we used bagging PLSR to conduct the predictions. Bagging aims to reduce the variance of predictions by aggregating a series of models obtained by resampling (Viscarra Rossel, 2007). We used bootstrap aggregation on the calibration data. This was completed by repeated random sampling with replacement  $B = 50$  times from the original data and produced 50 bootstrap samples. Each bootstrap sample has the same size as the original data with some replicates or part of the original data, and the remaining absent data are out-of-bag samples. The final prediction was the average of the 50 bootstrap models that we sampled. The uncertainties of the predictions were then calculated by their 95% confidence intervals (95% CIs).

$$\bar{f}(y) \pm 1.96 \times \sigma_{\bar{f}} \quad (2)$$

where  $\bar{f}(y)$  is the mean of the estimation from 50 bootstrap models, and  $\sigma_{\bar{f}}$  is the standard deviation of the estimation from 50 bootstrap

models.

## 2.7. Data analysis and assessment statistics

To achieve our objectives, we predicted the Cr content using the XRF and vis–NIR spectra. First, we predicted the Cr content using the XRF and vis–NIR spectra independently by PLSR and explored their prediction abilities using the VIP scores. Second, we estimated the Cr content using OPA fusion of the XRF and the vis–NIR spectra by PLSR and explored its mechanism using the VIP scores. Third, we estimated the Cr content using model averaging of PLSR predictions from the XRF and the vis–NIR spectra by GRA. Finally, we used bootstrapping to assess the uncertainties of the aforementioned prediction models.

We used a set of assessment criteria to compare the performance of the model predictions. The Lin's concordance correlation coefficient ( $\rho_c$ ) (Lin, 1989), which measures the precision and bias to determine how far predicted values deviate from the 1:1 line, was used to assess covariation and correspondence between the measured and the predicted values.  $\rho_c$  ranges from  $-1$  to  $1$ . The root mean square error of the prediction (RMSEP) and the ratio of prediction derivation (RPD) were used to quantify the accuracy of each prediction.

$$\rho_c = \frac{2 \times r \times s_{\hat{y}} \times s_y}{s_{\hat{y}}^2 + s_y^2 + (\bar{\hat{y}} - \bar{y})^2} \quad (3)$$

$$\text{RMSEP} = \sqrt{\frac{\sum_{i=1}^n (\hat{y}_i - y_i)^2}{n}} \quad (4)$$

$$\text{RPD} = \frac{\text{SD}}{\text{RMSEP}} \quad (5)$$

where  $y$  is the observed value and  $\hat{y}$  is the corresponding prediction;  $\bar{y}$  and  $\bar{\hat{y}}$  are the means of observed values and predictions, respectively; SD is the standard deviation;  $r$  is the usual Pearson product-moment correlation coefficient between the observed value and the prediction; and  $n$  is the sample number.

Additionally, we used the standard deviation of differences (SDD) to compare the spectral prediction error and the chemical measurement error. According to Peng et al. (2013),  $\text{RMSE} \leq 2 \times \text{SDD}$  is acceptable for many applications.

$$\text{SDD} = \sqrt{\frac{\sum (d_i - d_m)^2}{n - 1}} \quad (6)$$

where  $d_i$  is the difference in  $y$  between two replicates of sample  $i$ , and  $d_m$  is the mean of all replicate differences.

A good model has high  $\rho_c$  and RPD values and a low RMSEP. According to Viscarra Rossel and Hicks (2015),  $\rho_c$  value  $> 0.90$  indicates the model is excellent; value between  $0.80$  and  $0.90$  indicates the model is good, value between  $0.65$  and  $0.80$  indicates the model is moderate, and value  $< 0.65$  indicates the model is poor. If  $\text{RPD} > 2.0$ , the model is considered to be excellent. RPD value between  $1.4$  and  $2.0$  suggests the model can achieve approximate quantitative predictions, whereas value  $< 1.4$  indicates that the model is very poor (Chang et al., 2001). The procedure adopted in this study is depicted in Fig. 3.

## 3. Results

### 3.1. Soil Cr content

According to the Technical Specification for Soil Environmental Monitoring (HJ/T 166-2004) released by the Ministry of Ecology and Environment of the People's Republic of China ([http://kjs.mep.gov.cn/hjbhbz/bzwb/jcffbz/200412/t20041209\\_63367.shtml](http://kjs.mep.gov.cn/hjbhbz/bzwb/jcffbz/200412/t20041209_63367.shtml)), the maximum permissible relative deviations of the soil Cr measurement are dependent on the Cr content range in the soil (Table 1). The Cr content of all the soil samples measured in this study were between  $10$  and  $100 \text{ mg kg}^{-1}$  of soil and the maximum permissible relative deviation was  $\pm 10\%$ . All the

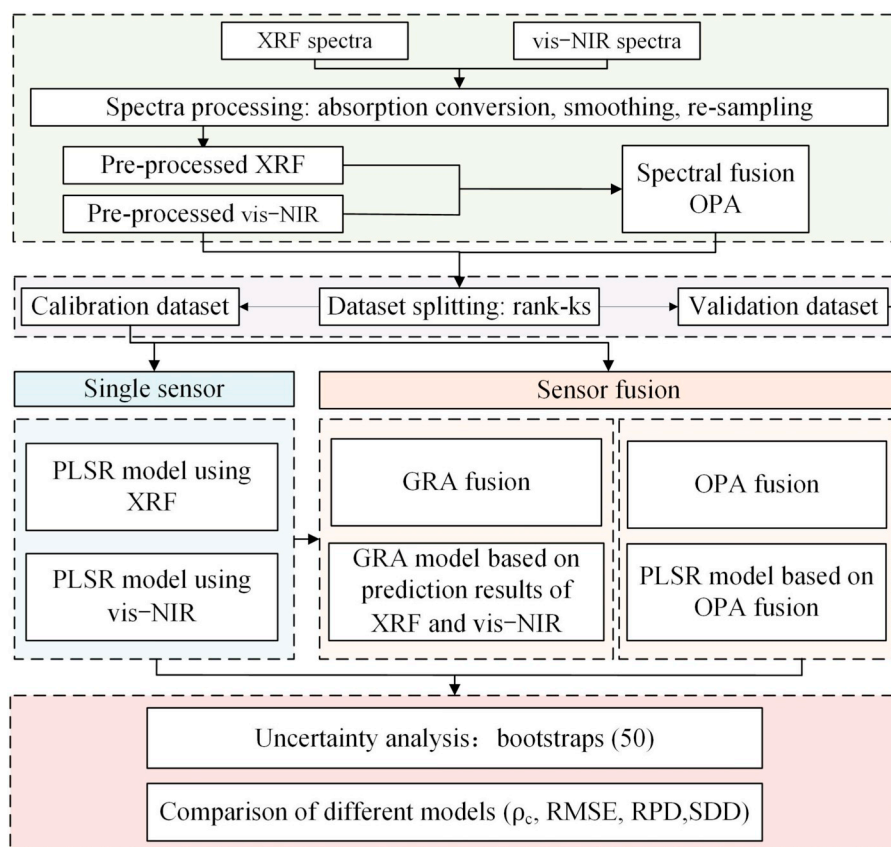


Fig. 3. Flowchart of the chemometric analysis.

Table 1

The maximum permissible relative deviation of two samples in soil monitoring according to the Technical Specification for soil Environmental monitoring (HJ/T 166-2004).

Content range (mg kg <sup>-1</sup> )	The maximum permissible relative deviation (%)
> 100	± 5
10–100	± 10
1.0–10	± 20
0.1–1.0	± 25
< 0.1	± 30

relative deviations of the measurements were lower than 10%, which confirmed the validity of the chemical analysis (Fig. 4).

The distributions of the calibration and validation datasets were similar to those of the whole dataset, which indicated that the split datasets were representative of the whole dataset. All datasets exhibited approximately normal distributions with skewness values close to 0 (Table 2). The Cr content varied between 10 and 80 mg kg<sup>-1</sup> of soil with a median of about 45 mg kg<sup>-1</sup> of soil and mean of about 43 mg kg<sup>-1</sup> of soil for the whole dataset.

### 3.2. Spectroscopic modelling of Cr content

Overall, soil Cr content was well predicted with confidence in all the methods tested in this study. A comprehensive list of the prediction accuracies of calibration and validation using XRF, vis-NIR, OPA, and GRA is presented in Table 3. For the single sensor assessment, XRF performed better than vis-NIR. The  $\rho_c$  values were 0.83 and 0.80 for the validation samples using the XRF and the vis-NIR spectra, respectively. The RPD values for the XRF and the vis-NIR spectra were 1.75 and 1.63, respectively. Among the single and combined sensor assessments, OPA fusion of XRF and vis-NIR performed the best with  $\rho_c$  of 0.90 and RPD

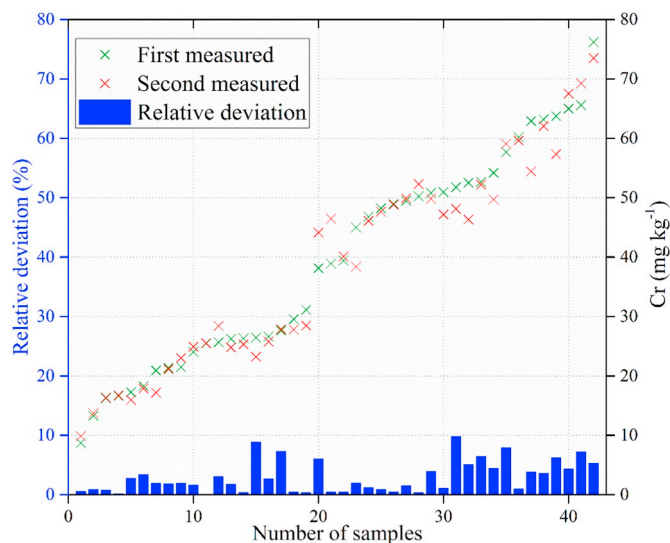


Fig. 4. Cr content in the soil samples including the results of repeated measurements and their relative deviation. The red and green cross are the result of first and second measurements, respectively and the blue bar is the relative deviation of the two measurements. (For interpretation of the references to color in this figure legend, the reader is referred to the web version of this article.)

of 2.30 for the validation dataset. The GRA model performed better than the single sensors and was comparable to the OPA fusion with a  $\rho_c$  of 0.88 and RPD of 2.13 for the validation dataset.

Fig. 5 shows the prediction performances of the four models constructed using single sensors and sensor fusion, along with their prediction uncertainties. Among these models, the prediction model using OPA

**Table 2**  
Descriptive statistics of Cr (in  $\text{mg kg}^{-1}$ ) measured by ICP-MS in the laboratory.

Dataset	N	Min.	1st Q.	Median	Mean	3rd Q.	Max.	Skewness
All	291	9.865	18.82	44.84	43.04	54.36	80.64	-0.24
Calibration	194	9.865	18.82	44.84	43	54.42	80.07	-0.28
Validation	97	13.05	18.81	45.47	43.13	54.25	80.64	-0.17

**Table 3**  
Comparison of prediction accuracy of different methods (all values are the mean of 50 bootstraps).

Approach	Calibration			Validation		
	$\rho_c$	RMSE	RPD	$\rho_c$	RMSE	RPD
XRF	0.95	4.79	3.26	0.83	8.80	1.75
Vis-NIR	0.94	5.20	2.96	0.80	9.47	1.63
OPA	0.98	3.27	4.65	0.90	6.80	2.30
GRA	0.96	3.98	3.86	0.88	7.40	2.13

fusion performed the best. The  $\rho_c$  value for the validation dataset by the OPA approach was 0.90, with 95% CIs from 0.88 to 0.93, and the RPD value was 2.30 with its corresponding 95% CIs between 1.91 and 2.68. The second-best performance was achieved with the GRA model with a  $\rho_c$  value of 0.88 (95% CIs between 0.85 and 0.90) and RPD of 2.13 (95% CIs between 1.90 and 2.37). These results clearly showed excellent agreement between the measured Cr content and the OPA and GRA predictions. Prediction using the XRF spectra showed good agreement with the Cr content. For example, the  $\rho_c$  and RPD values of the prediction were 0.83 (95% CIs from 0.78 to 0.89) and 1.75 (95% CIs from 1.42 to 2.08).

**Table 4**  
comparison between chemical measurement error and spectra prediction error.

Index	Instrument	Value ( $\text{mg kg}^{-1}$ )
SDD	ICP_MS	4.23
RMSEP	XRF	8.80
	Vis-NIR	9.47
	OPA	6.80
	GRA	7.40

For vis-NIR spectra, the  $\rho_c$  and RPD values were 0.80 and 1.63, respectively. Their 95% CIs were from 0.76 to 0.84 and 1.38 to 1.87, respectively. These results indicated relatively weaker performance of vis-NIR spectra than XRF spectra in predicting soil Cr content.

Chemical measurement errors and spectral prediction errors were compared by calculating SDD of the replicated chemical measurements and the RMSEP of the spectra (Table 4). The RMSEP of OPA and GRA were  $6.80 \text{ mg kg}^{-1}$  and  $7.40 \text{ mg kg}^{-1}$ , respectively, and were  $< 2 \times \text{SDD}$  ( $8.46 \text{ mg kg}^{-1}$ ). This indicated that the predictions using OPA and GRA were acceptable for these applications. By contrast, the RMSEP of single sensor predictions were larger than  $2 \times \text{SDD}$  and questioned the validity of the approaches for this application. The predictions obtained through fusion of data from multiple sensors were superior to those obtained using data from single sensors.

### 3.3. Variable importance projection analysis for the three approaches

The VIP scores for PLSR models of the XRF and the vis-NIR spectra are shown in Fig. 6. For XRF, there were high VIP scores of  $> 1.0$  at around 5.5–7.0, 12.9–14.5, and 15.0–17.0 keV. Especially for the energy around 5.9 and 16.0 keV, the VIP scores were larger than 3.0. There were

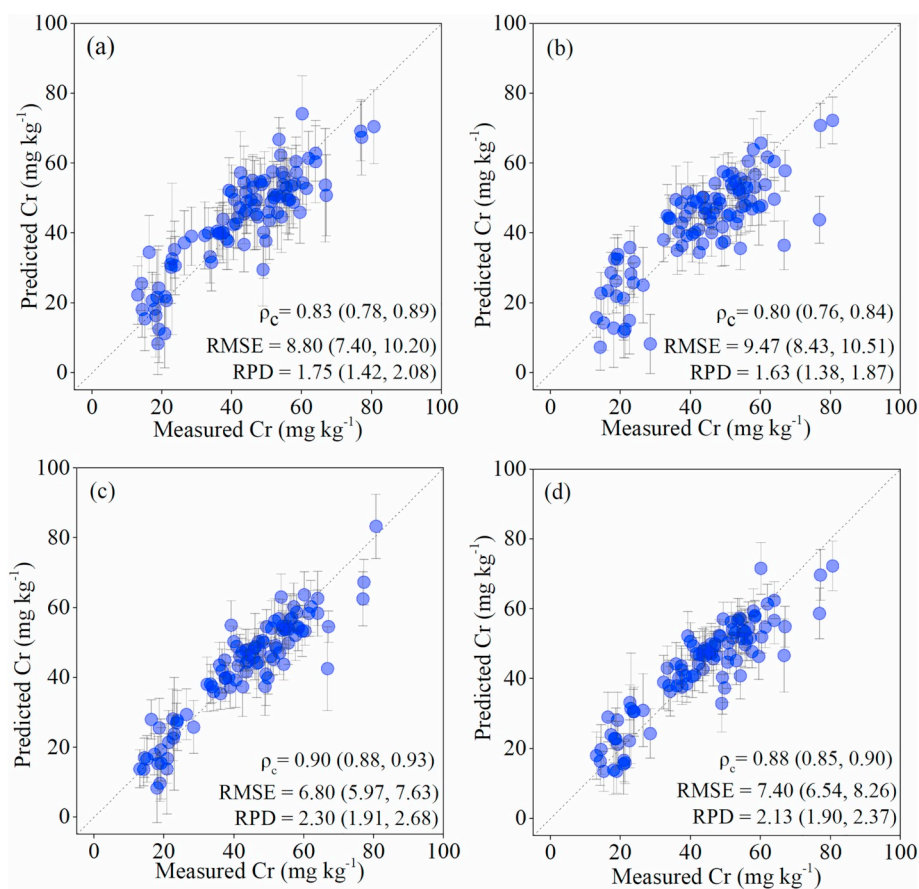


**Fig. 5.** Performance for validation of four models (a) XRF model, (b) vis-NIR model, (c) OPA model (d) GRA model. The light grey bars represent the 95% confidence intervals derived from bootstrapping and the dotted line shows the 1:1 relationship. The values in parentheses represents 95% confidence intervals (CIs).

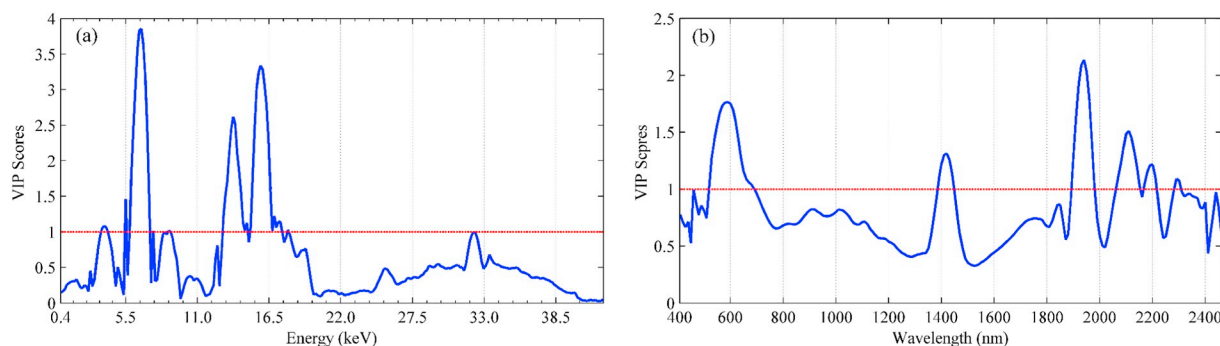


Fig. 6. VIP scores of the Cr predictions for single sensors, (a) XRF and (b) vis-NIR.

small peaks at 3.5, 5.5, 8.7, 17.2, 18.0, and 32.0 keV with VIP scores around 1.0. For vis-NIR, VIP scores of > 1.0 were observed at around 470, 517–673, 1379–1424, 1891–1967, 2058–2144, 2160–2174, 2184–2214, 2222–2231, and 2331–2358 nm. Among these, large peaks were observed at around 470, 577, 1413, 1910, 2120, 2166, 2206, 2226, and 2344 nm. Unlike the single instruments results, the VIP scores of OPA fusion using both XRF and vis-NIR spectra need to be presented in three-dimensional color contour graphs (Fig. 7). The VIP scores for the XRF energies around 5.5–7.0, 12.9–14.5, and 15.0–17.0 keV were larger than 6.0 for almost all the wavelengths of the vis-NIR spectra. The vis-NIR had large VIP scores around 1410, 1910, 2200, and 2300 nm and these intersected with the energies of XRF. These high VIP scores of the OPA were higher than the VIP scores of the individual XRF and vis-NIR spectra. The highest VIP scores were > 9. Similarly, in the OPA matrix, the XRF also showed larger VIP scores than vis-NIR, perhaps because of the direct relationship with the Cr content.

## 4. Discussion

### 4.1. Predictions using a single sensor

As a suitable alternative to traditional analysis for the measurement of soil heavy metal content, XRF has gained increasing popularity, especially for the measurement of Pb, Cu, Zn, Cd, and Cr (Rouillon and Taylor, 2016). And previous study mainly used XRF elemental data, while when the heavy metal contents were in low concentrations, the elemental data would be failed to be detected because of LODs.

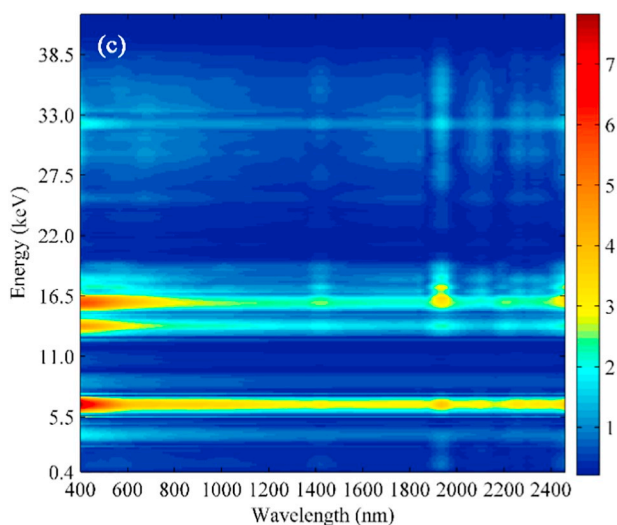


Fig. 7. VIP scores of the Cr predictions for OPA fusion. X-axis represents the wavelengths of vis-NIR spectra and the Y-axis represents the energy of XRF spectra.

According to O'Rourke et al. (2016), compared with XRF elemental concentrations, XRF spectra was more effective for determination of elements present in low concentrations. Thus, in these cases, we could consider to use the raw spectra of XRF to develop spectral calibration models. In this study, we used XRF spectra to predict soil Cr content and obtained moderate to good results (Table 3 and Fig. 5). These results were comparable with those from previous studies by Moros et al. (2010) and Hseu et al. (2016). XRF measures the energy levels of X-rays emitted from Cr, which has a characteristic binding energy (McLaren et al., 2012). Our results were also in line with previous studies (Moros et al., 2010; McLaren et al., 2012) that indicated that the absorption energy of Cr was mainly located between 5–7 keV (Fig. 6). High VIP scores at 12.9–14.5 and 15.0–17.0 keV indicated that prediction may be attributable to the influences of other elements. There was large uncertainty in the prediction of Cr content using XRF spectra (Fig. 5). Some previous studies also reported this issue. These may be attributable to large differences in the sites and their Cr content. For example, Caporale et al. (2018) predicted Cr content using XRF in two case studies and reported  $R^2$  of 0.95 and 0.54.

The prediction of Cr content using vis-NIR spectra was slightly worse than the prediction using XRF spectra (Table 3 and Fig. 5). This was on par with previous research on determination of soil organic and inorganic elements using XRF and vis-NIR spectra (O'Rourke et al., 2016). However, the prediction uncertainty using the vis-NIR spectra was slightly smaller than that of the XRF spectra. Soil heavy metals are often bound to soil organic matter and clay minerals (Choe et al., 2008; Chen et al., 2015; Shi et al., 2016), which are related to carbonates, hydroxides, or oxides that have spectrally active components in the vis-NIR region (Stenberg et al., 2010; Araujo et al., 2014). For example, in the visible region, the high VIP scores for Cr were mainly in the 470–580 nm region (Fig. 6), which is related to soil organic matter (Shi et al., 2015; Xu et al., 2018). Another region of high VIP scores was at around 1413 nm and 1910 nm, which is mainly related to O–H bonds in water or clay minerals. High VIP scores at around 2120, 2166, 2206, 2226, and 2344 nm were associated with Al–OH and O–H in clay minerals, such as kaolinite, montmorillonite, and illite (Viscarra Rossel and Behrens, 2010; Song et al., 2013).

### 4.2. Predictions using sensor fusion

The prediction using OPA fusion was better than the predictions from the single sensors in terms of accuracy and uncertainty. This indicates that the OPA fusion combining XRF and vis-NIR spectra is an efficient approach for Cr content prediction (Table 3 and Fig. 5). Compared with previous studies that used OPA to fuse vis-NIR and mid-IR spectra (Cecillon et al., 2012; Terra et al., 2019), this study achieved an obvious improvement in fusing XRF and vis-NIR spectra for Cr prediction. This may be because we used different energies for the spectra, which meant the OPA made full use of their distinct natures and complementary information. Moreover, the distribution of VIP scores for the fused spectra had a similar trend to those of the individual

**Table 5**  
Weights assigned to XRF and vis-NIR in GRA.

Sensor	XRF	Vis-NIR
Weights	0.56	0.48
95% CIs	(0.37, 0.74)	(0.29, 0.68)

spectra, but the XRF spectra played a more important role than vis-NIR in the PLSR model (Fig. 7). Thus, compared with a simple concatenation of different spectra, OPA expands the possibility of finding spectral co-evolutions that are highly associated with Cr (Barros et al., 2008; Terra et al., 2019). The OPA of XRF and vis-NIR spectra provides an effective and stable approach for Cr prediction.

Model averaging improves the model prediction accuracy more consistently than individual sensor models (Malone et al., 2014; Xu et al., 2019). Previous studies have proved that GRA is an efficient and simple method that only requires fitting to a simple linear regression model (Malone et al., 2014; O'Rourke et al., 2016). Therefore, we used GRA to conduct model averaging to realize sensor fusion. The results were also in line with previous studies (Table 3 and Fig. 5). XRF prediction was preferred over vis-NIR for Cr prediction (Table 5), and this was comparable to the results from O'Rourke et al. (2016) (Fig. 7). Compared with the predictions using individual sensors, the predictions using OPA and GRA provided more satisfactory results (for  $\rho_c$ , RPD, RMSE, and SDD) (Table 4 and Fig. 5). Overall, the sensor fusion of vis-NIR and XRF with OPA and GRA provided similar results and can be recommended for Cr estimation.

Although it takes extra time and is costlier, sensor fusion approach provides more accurate and stable prediction model for soil properties (Table 3 and Fig. 5) (Wang et al., 2015; O'Rourke et al., 2016; Xu et al., 2019). With rapid technical development, more advanced and affordable soil sensors will be available in future. Recently, there have been some attempts to develop soil sensing platforms, such as the soil condition analysis system (Viscarra Rossel et al., 2017), and the project '14S-Integrated system for site-specific soil fertility management'. These multi-sensor platforms aim to detect various soil properties simultaneously, and sensor fusion has high potential to improve the stability of stable estimates. In future study, we will try to use the sensor fusion approach to estimate other soil properties or element content.

## 5. Conclusions

In overcoming challenges associated with the traditional measurements of heavy metals, including Cr, soil spectroscopy has attracted tremendous attention. Although the technology has developed rapidly, spectral data processing still presents challenges, particularly, when complementary information from multiple sensors is used to improve the predictions. In this study, we used XRF and vis-NIR individually and in combination to predict soil Cr content in paddy soils from China. We used two sensor fusion approaches, OPA and GRA, to combine the data from the XRF and vis-NIR for the prediction of soil Cr content. For single sensor, XRF had better prediction accuracy but larger prediction uncertainty than vis-NIR. Among the single and combined sensors, OPA fusion of XRF and vis-NIR spectra provided the best prediction with the largest  $\rho_c$  and RPD and the smallest RMSE and uncertainty. Sensor fusion by GRA was comparable to OPA fusion, and the OPA and GRA gave acceptable SDD values. Thus, this study provides a recommendation to use either OPA or GRA fusion of XRF and vis-NIR data for the predictions of soil Cr content.

## Acknowledgements

We thank the support of the National Key Research and Development Program (2018YFC1800105).

## References

- Araujo, S.R., Dematte, J.A.M., Vicente, S., 2014. Soil contaminated with chromium by tannery sludge and identified by vis-NIR-mid spectroscopy techniques. *Int. J. Remote Sens.* 35 (10), 3579–3593.
- Argyaki, A., Ramsey, M.H., Potts, P.J., 1997. Evaluation of portable X-ray fluorescence instrumentation for in situ measurements of lead on contaminated land. *Analyst* 122 (8), 743–749.
- Barros, A.S., Pinto, R., Bouveresse, D.J.R., Rutledge, D.N., 2008. Principal component transform–outer product analysis in the PCA context. *Chemom. Intell. Lab. Syst.* 93 (1), 43–48.
- Baveye, P.C., Laba, M., 2015. Visible and near-infrared reflectance spectroscopy is of limited practical use to monitor soil contamination by heavy metals. *J. Hazard. Mater.* 285, 137–139.
- Caporale, A.G., Adamo, P., Capozzi, F., Langella, G., Terribile, F., Vingiani, S., 2018. Monitoring metal pollution in soils using portable-XRF and conventional laboratory-based techniques: evaluation of the performance and limitations according to metal properties and sources. *Sci. Total Environ.* 643, 516–526.
- Cecillon, L., Certini, G., Lange, H., Forte, C., Strand, L.T., 2012. Spectral fingerprinting of soil organic matter composition. *Org. Geochem.* 46, 127–136.
- Chakraborty, S., Weindorf, D.C., Deb, S., Li, B., Paul, S., Choudhury, A., Ray, D.P., 2017. Rapid assessment of regional soil arsenic pollution risk via diffuse reflectance spectroscopy. *Geoderma* 289, 72–81.
- Chang, C.W., Laird, D.A., Mausbach, M.J., Hurburgh, C.R., 2001. Near-infrared reflectance spectroscopy-principal components regression analyses of soil properties. *Soil Sci. Soc. Am. J.* 65 (2), 480–490.
- Chen, T., Chang, Q., Clevers, J.G.P.W., Koistra, L., 2015. Rapid identification of soil cadmium pollution risk at regional scale based on visible and near-infrared spectroscopy. *Environ. Pollut.* 206, 217–226.
- Chen, S., Peng, J., Ji, W., Zhou, Y., He, J., Shi, Z., 2016. Study on the characterization of VNIR-MIR spectra and prediction of soil organic matter in paddy soil. *Spectrosc. Spectr. Anal.* 36 (6), 1712–1716.
- Chen, S., Li, S., Ma, W., Ji, W., Xu, D., Shi, Z., Zhang, G., 2019a. Rapid determination of soil classes in soil profiles using vis-NIR spectroscopy and multiple objectives mixed support vector classification. *Eur. J. Soil Sci.* 70, 42–53.
- Chen, S., Liang, Z., Webster, R., Zhang, G., Zhou, Y., Teng, H., 2019b. A high-resolution map of soil pH in China made by hybrid modelling of sparse soil data and environmental covariates and its implications for pollution. *Sci. Total Environ.* 655, 273–283.
- Choe, E., van der Meer, F., van Ruitenbeek, F., van der Werff, H., de Smeth, B., Kim, Y.-W., 2008. Mapping of heavy metal pollution in stream sediments using combined geochemistry, field spectroscopy, and hyperspectral remote sensing: a case study of the Rodalquilar mining area, SE Spain. *Remote Sens. Environ.* 112 (7), 3222–3233.
- Di Palma, L., Gueye, M.T., Petrucci, E., 2015. Hexavalent chromium reduction in contaminated soil: a comparison between ferrous sulphate and nanoscale zero-valent iron. *J. Hazard. Mater.* 281, 70–76.
- Ellis, A.S., Johnson, T.M., Bullen, T.D., 2002. Chromium isotopes and the fate of hexavalent chromium in the environment. *Science* 295 (5562), 2060–2062.
- Fernández, P.M., Figueroa, L.I.C., Farina, J.I., 2010. Critical influence of culture medium and Cr(III) quantification protocols on the interpretation of Cr(VI) bioremediation by environmental fungal isolates. *Water Air Soil Pollut.* 206 (1–4), 283–293.
- Gao, Y., Xia, J., 2011. Chromium contamination accident in China: viewing environment policy of China. *Environ. Sci. Technol.* 45 (20), 8605–8606.
- Gong, Z.T., Zhang, G.L., Chen, Z.C., 2007. *Pedogenesis and Soil Taxonomy*. Science Press, Beijing.
- Granger, C.W.J., Ramanathan, R., 1984. Improved methods of combining forecasts. *J. Forecast.* 3, 197–204.
- Horta, A., Malone, B., Stockmann, U., Minasny, B., Bishop, T.F.A., McBratney, A.B., Pallasser, R., Pozza, L., 2015. Potential of integrated field spectroscopy and spatial analysis for enhanced assessment of soil contamination: a prospective review. *Geoderma* 241, 180–209.
- Hou, X., He, Y., Jones, B.T., 2004. Recent advances in portable X-ray fluorescence spectrometry. *Appl. Spectrosc. Rev.* 39 (1), 1–25.
- Hseu, Z.Y., Chen, Z.S., Tsai, C.C., Jien, S.H., 2016. Portable X-ray fluorescence (pXRF) for determining Cr and Ni contents of serpentine soils in the field. In: Hartemink, A.E., Minasny, B. (Eds.), *Digital Soil Morphometrics. Progress in Soil Science*, pp. 37–50.
- Jaillais, B., Pinto, R., Barros, A.S., Rutledge, D.N., 2005. Outer-product analysis (OPA) using PICA to study the influence of temperature on NIR spectra of water. *Vib. Spectrosc.* 39 (1), 50–58.
- Jaillais, B., Ottenhof, M.A., Farhat, I.A., Rutledge, D.N., 2006. Outer-product analysis (OPA) using PLS regression to study the retrogradation of starch. *Vib. Spectrosc.* 40 (1), 10–19.
- Ji, W., Rossel, R.A.V., Shi, Z., 2015. Improved estimates of organic carbon using proximally sensed vis-NIR spectra corrected by piecewise direct standardization. *Eur. J. Soil Sci.* 66 (4), 670–678.
- Juvera-Espinosa, J., Morales-Barrera, L., Cristiani-Urbina, E., 2006. Isolation and characterization of a yeast strain capable of removing Cr(VI). *Enzym. Microb. Technol.* 40 (1), 114–121.
- Kemper, T., Sommer, S., 2002. Estimate of heavy metal contamination in soils after a mining accident using reflectance spectroscopy. *Environ. Sci. Technol.* 36 (12), 2742–2747.
- Kennard, R.W., Stone, L.A., 1969. Computer aided design of experiments. *Technometrics* 11, 137–148.
- Lin, L.I., 1989. A concordance correlation-coefficient to evaluate reproducibility. *Biometrics* 45 (1), 255–268.

- Malone, B.P., Minasny, B., Odgers, N.P., McBratney, A.B., 2014. Using model averaging to combine soil property rasters from legacy soil maps and from point data. *Geoderma* 232, 34–44.
- McLaren, T.L., Guppy, C.N., Tighe, M.K., Forster, N., Grave, P., Lisle, L.M., Bennett, J.W., 2012. Rapid, nondestructive total elemental analysis of vertisol soils using portable X-ray fluorescence. *Soil Sci. Soc. Am. J.* 76 (4), 1436–1445.
- Mevik, B.H., Wehrens, R., 2016. Pls: Partial Least Squares and Principal Component Regression, R Package Version 2.6–0. (WWWdocument).
- Moros, J., Gredilla, A., Fdez-Ortiz de Vallejuelo, S., de Diego, A., Manuel Madariaga, J., Garrigues, S., de la Guardia, M., 2010. Partial least squares X-ray fluorescence determination of trace elements in sediments from the estuary of Nerbioi-Ibaizabal River. *Talanta* 82 (4), 1254–1260.
- Naesset, E., Bollandsas, O.M., Gobakken, T., 2005. Comparing regression methods in estimation of biophysical properties of forest stands from two different inventories using laser scanner data. *Remote Sens. Environ.* 94 (4), 541–553.
- O'Rourke, S.M., Stockmann, U., Holden, N.M., McBratney, A.B., Minasny, B., 2016. An assessment of model averaging to improve predictive power of portable vis-NIR and XRF for the determination of agronomic soil properties. *Geoderma* 279, 31–44.
- Peng, Y., Knadel, M., Gislum, R., Deng, F., Norgaard, T., de Jonge, L.W., Moldrup, P., Greve, M.H., 2013. Predicting soil organic carbon at field scale using a national soil spectral library. *J. Near Infrared Spectrosc.* 21 (3), 213–222.
- Piccolo, A., Stevenson, F.J., 1982. Infrared-spectra of Cu-2+, Pb-2+, and Ca-2+ complexes of soil humic substances. *Geoderma* 27 (3), 195–208.
- R Core Team, 2017. R: A Language and Environment for Statistical Computing. R Foundation for Statistical Computing, Vienna [WWWdocument]. URL: <https://www.R-project.org/>, Accessed date: 6 March 2017.
- Reidinger, S., Ramsey, M.H., Hartley, S.E., 2012. Rapid and accurate analyses of silicon and phosphorus in plants using a portable X-ray fluorescence spectrometer. *New Phytol.* 195 (3), 699–706.
- Rojas, R., Feyen, L., Dassargues, A., 2008. Conceptual model uncertainty in groundwater modeling: combining generalized likelihood uncertainty estimation and Bayesian model averaging. *Water Resour. Res.* 44 (12).
- Rouillon, M., Taylor, M.P., 2016. Can field portable X-ray fluorescence (pXRF) produce high quality data for application in environmental contamination research? *Environ. Pollut.* 214, 255–264.
- Savitzky, A., Golay, M.J.E., 1964. Smoothing and differentiation of data by simplified least squares procedures. *Anal. Chem.* 36 (8), 1627–1639.
- Shi, T.Z., Liu, H.Z., Wang, J.J., Chen, Y.Y., Fei, T., Wu, G.F., 2014. Monitoring arsenic contamination in agricultural soils with reflectance spectroscopy of rice plants. *Environ. Sci. Technol.* 48 (11), 6264–6272.
- Shi, Z., Ji, W., Rossel, R.A.V., Chen, S., Zhou, Y., 2015. Prediction of soil organic matter using a spatially constrained local partial least squares regression and the Chinese vis-NIR spectral library. *Eur. J. Soil Sci.* 66 (4), 679–687.
- Shi, T.Z., Wang, J.J., Chen, Y.Y., Wu, G.F., 2016. Improving the prediction of arsenic contents in agricultural soils by combining the reflectance spectroscopy of soils and rice plants. *Int. J. Appl. Earth Obs. Geoinf.* 52, 95–103.
- Song, Y.X., Ji, J.F., Mao, C.P., Ayoko, G.A., Frost, R.L., Yang, Z.F., Yuan, X.Y., 2013. The use of reflectance visible-NIR spectroscopy to predict seasonal change of trace metals in suspended solids of Changjiang River. *Catena* 109, 217–224.
- Stenberg, B., Viscarra Rossel, R.A., Mouazen, A.M., Wetterlind, J., 2010. Visible and near infrared spectroscopy in soil science. *Adv. Agron.* 107, 163–215.
- Sun, W., Zhang, X., Sun, X., Sun, Y., Cen, Y., 2018. Predicting nickel concentration in soil using reflectance spectroscopy associated with organic matter and clay minerals. *Geoderma* 327, 25–35.
- Terra, F.S., Viscarra Rossel, R.A., Dematté, J.A.M., 2019. Spectral fusion by Outer Product Analysis (OPA) to improve predictions of soil organic C. *Geoderma* 335, 35–46.
- Vesela, A., Barros, A.S., Synytsya, A., Delgado, I., Copikova, J., Coimbra, M.A., 2007. Infrared spectroscopy and outer product analysis for quantification of fat, nitrogen, and moisture of cocoa powder. *Anal. Chim. Acta* 601 (1), 77–86.
- Viscarra Rossel, R., 2007. Robust modelling of soil diffuse reflectance spectra by bagging-partial least squares regression. *J. Near Infrared Spectrosc.* 15 (2), 39.
- Viscarra Rossel, R.A., Behrens, T., 2010. Using data mining to model and interpret soil diffuse reflectance spectra. *Geoderma* 158 (1–2), 46–54.
- Viscarra Rossel, R.A., Hicks, W.S., 2015. Soil organic carbon and its fractions estimated by visible-near infrared transfer functions. *Eur. J. Soil Sci.* 66 (3), 438–450.
- Viscarra Rossel, R.A., Walvoort, D.J.J., McBratney, A.B., Janik, L.J., Skjemstad, J.O., 2006. Visible, near infrared, mid infrared or combined diffuse reflectance spectroscopy for simultaneous assessment of various soil properties. *Geoderma* 131 (1–2), 59–75.
- Viscarra Rossel, R.A., Behrens, T., Ben-Dor, E., 2016. A global spectral library to characterize the worlds soil. *Earth-Sci. Rev.* 155, 198–230.
- Viscarra Rossel, R.A., Lobsey, C.R., Sharman, C., Flick, P., McLachlan, G., 2017. Novel proximal sensing for monitoring soil organic C stocks and condition. *Environ. Sci. Technol.* 51 (10), 5630–5641.
- Wang, D., Chakraborty, S., Weindorf, D.C., Li, B., Sharma, A., Paul, S., Ali, M.N., 2015. Synthesized use of VisNIR DRS and PXRF for soil characterization: Total carbon and total nitrogen. *Geoderma* 243–244, 157–167.
- Wold, S., Martens, H., Wold, H., 1983. The multivariate calibration-problem in chemistry solved by the PLS method. *Lect. Note Math.* 973, 286–293.
- Wold, S., Sjostrom, M., Eriksson, L., 2001. PLS-regression: a basic tool of chemometrics. *Chemom. Intell. Lab. Syst.* 58 (2), 109–130.
- Xu, D., Ma, W., Chen, S., Jiang, Q., He, K., Shi, Z., 2018. Assessment of important soil properties related to Chinese Soil Taxonomy based on vis-NIR reflectance spectroscopy. *Comput. Electron. Agric.* 144, 1–8.
- Xu, D., Zhao, R., Li, S., Chen, S., Jiang, Q., Zhou, L., Shi, Z., 2019. Multi-sensor fusion for the determination of several soil properties in the Yangtze River Delta, China. *Eur. J. Soil Sci.* 70, 162–173.
- Zhu, Y., Weindorf, D.C., Zhang, W., 2011. Characterizing soils using a portable X-ray fluorescence spectrometer: 1. Soil texture. *Geoderma* 167–68, 167–177.